Published in final edited form as:
Nanomedicine (Lond). 2011 October ; 6(8): 1341–1352. doi:10.2217/nnm.11.37.

Development of iron-containing multiwalled carbon nanotubes for MR-guided laser-induced thermotherapy

Xuanfeng Ding[1,2], **Ravi Singh**[2], **Andrew Burke**[2], **Heather Hatcher**[2], **John Olson**[2], **Robert A Kraft**[2], **Michael Schmid**[1], **David Carroll**[1,3], **J Daniel Bourland**[1,2,3], **Steven Akman**[2,3], **Frank M Torti**[2,3], and **Suzy V Torti**[2,3,†]

[1]Wake Forest University, Winston Salem, NC 27106, USA

[2]Wake Forest University School of Medicine, Winston, Salem, NC 275157, USA

[2]Comprehensive Cancer Center, Wake Forest University School of Medicine, Winston Salem, NC 27157, USA

Abstract

Aims—To test iron-containing multiwalled carbon nanotubes (MWCNTs) as bifunctional nanomaterials for imaging and thermal ablation of tumors.

Materials & Methods—MWCNTs entrapping iron were synthesized by chemical vapor deposition. The T2-weighted contrast enhancement properties of MWCNTs containing increasing amounts of iron were determined *in vitro*. Suspensions of these particles were injected into tumor-bearing mice and tracked longitudinally over 7 days by MRI. Heat-generating abilities of these nanomaterials following exposure to near infrared (NIR) laser irradiation was determined *in vitro* and *in vivo*.

Results—The magnetic resonance contrast properties of carbon nanotubes were directly related to their iron content. Iron-containing nanotubes were functional T2-weighted contrast agents *in vitro* and could be imaged *in vivo* long-term following injection. Iron content of nanotubes did not affect their ability to generate thermoablative temperatures following exposure to NIR and significant tumor regression was observed in mice treated with MWCNTs and NIR laser irradiation.

Conclusion—These data demonstrate that iron-containing MWCNTs are functional T2-weighted contrast agents and efficient mediators of tumor-specific thermal ablation *in vivo*.

Keywords

cancer; contrast agent; *in vivo*; laser; MRI; nanotube; T2; thermal therapy

[†]Author for correspondence: Tel.: +1 336 716 9357, Fax: +1 336 716 0255, storti@wfubmc.edu.

Financial & competing interests disclosure
The authors have no other relevant affiliations or financial involvement with any organization or entity with a financial interest in or financial conflict with the subject matter or materials discussed in the manuscript apart from those disclosed.
No writing assistance was utilized in the production of this manuscript.

Ethical conduct of research
The authors state that they have obtained appropriate institutional review board approval or have followed the principles outlined in the Declaration of Helsinki for all human or animal experimental investigations. In addition, for investigations involving human subjects, informed consent has been obtained from the participants involved.

Biomedical applications of nanomaterials will provide a valuable set of tools and devices for both research and clinical purposes [1]. Among the diversity of investigational nanomaterials, carbon nanotubes (CNTs) have attracted substantial attention due to a combination of features that make them useful for biomedical applications. They can be easily internalized by cells [2–4] and can therefore act as delivery vehicles for a variety of molecules relevant to therapy and diagnosis of disease [5]. Moreover, their unique combination of electrical, thermal and spectroscopic properties offers further opportunities for advances in the detection, monitoring and therapy of diseases, especially cancer [6–12].

One promising application of nanomaterials for the treatment of disease has been as heat transduction agents for laser-induced thermotherapy (LITT) of cancer [13]. LITT is a thermal ablation technique that uses laser radiation to deliver energy to a target tissue, such as a tumor, to induce heating above the thermal ablation temperature threshold of approximately 55°C [13–15]. As a result of heating, protein denaturation, membrane lysis and coagulative necrosis occur, leading to cell death. LITT offers many advantages over other modalities of thermal therapy, such as radiofrequency (RF) or microwave ablation [6,16–18]. These include the compatibility of fiber optic laser instruments with magnetic resonance (MR) thermometry [19], which allows for precise monitoring of treatment temperatures, ensuring effective treatment of the target lesion while limiting injury to adjacent healthy tissue. By contrast, due to its instrumentation requirements, RF treatment is largely incompatible with simultaneous MRI. Furthermore, the laser beam delivering the near infrared (NIR) radiation can, in principle, be shaped to provide a relatively even fluence distribution of irradiation to the tumor volume. Probes used for RF ablation are typically point sources and do not possess such a degree of flexibility in shaping the treatment volume.

Despite its advantages, the clinical utility of LITT has been limited by an inability to consistently achieve thermoablative temperatures throughout the target lesion and to confine treatment exclusively to the tumor. Earlier efforts to address these deficiencies involved injecting tumors with light-absorbing dyes to promote tumor-specific heating; however, low heat transduction efficiency has limited their use [20,21]. By contrast, nanoparticles can be engineered as high-efficiency absorbers of tuned, laser radiation and promote the generation of therapeutic heat, specifically in tumors where they have been injected [19]. We have recently demonstrated that multiwalled carbon nanotubes (MWCNTs) heated by laser-emitted NIR are effective agents for localizing LITT to a tumor site [19]. We also demonstrated that MR thermometry could be used to assess temperature increase in tumors and calculate the delivered thermal dose to that same tissue following MWCNT-mediated LITT [19]. Development of a MWCNT that retains the ability to serve as a heat transducer for LITT and also functions as an MR contrast agent would confer an additional advantage by allowing the intratumoral distribution of the nanomaterial to be imaged prior to treatment, facilitating pretreatment planning and image-guided therapy. In this article, we tested whether MWCNTs that incorporate iron, a known MRI contrast agent, could be used for this purpose.

The strategy of using iron-containing MWCNTs for simultaneous thermal therapy and MR imaging was based on several considerations. First, we selected MWCNTs based on their superior thermal ablation properties relative to single-walled carbon nanotubes (SWCNTs) [19], which are also being explored as MR contrast agents [22]. Second, we used iron as the MR contrast agent because iron is a well-known T2 contrast agent for MR imaging [23–28]. Third, we elected to entrap the iron within the MWCNT rather than place it on the surface to avoid potential toxicities of surface iron, as well as to avoid potential interference of covalent functionalization with the electrical and thermal properties of the MWCNT.

In this article, we demonstrate that chemical vapor deposition synthesized MWCNTs entrap iron in proportion to the mass of ferrocene present during synthesis and that such nanotubes are effective MR contrast agents *in vitro* and *in vivo*. Furthermore, iron entrapment does not interfere with MWCNTs efficacy as transducers for LITT. Use of a dual-modality nanoparticle that is capable of being located by MRI and is also effective as a mediator of LITT may overcome some of the drawbacks of traditional thermotherapy.

Experimental methods

Materials

Iron-containing MWCNTs were produced by pyrolysis of ferrocene onto silica substrates at the Wake Forest University Center for Nanotechnology and Molecular Materials (NC, USA). The synthesis apparatus consisted of a two-stage tubular quartz furnace: the first stage was the preheater (maintained at 160°C) and the second was the growth oven (maintained at 600–900°C). Ferrocene (60, 200, 400 or 600 mg) was dissolved in 10 ml of xylene and the mixture was vaporized at 700°C. The ferrocene vapor was injected into the preheater stage of the furnace using a syringe pump with a feed rate of 5 ml/h. Through the thermal decomposition of ferrocene, iron catalyst particles were deposited on the furnace wall and substrate surfaces, forming the base for MWCNT growth. Carbon vapor with hydrogen as a carrier gas and a flow rate of 320 cm^3/min was then introduced; the growth time for MWCNT synthesis was approximately 1 h. During this synthesis, a small fraction of iron particles become entrapped in the nanotubes. MWCNTs were collected from the central portion of the oven growth zone and cleaned by ultrasonication in sulfuric and nitric acid (3:1) for 20 h. Purified iron-containing MWCNTs were massed and suspended in saline with 1% (wt/wt) pluronic F127 (Sigma, MO, USA) by sonication and imaged using a Philips 400 transmission electron microscope. Iron content was measured by Huffman Laboratories (CO, USA).

Measurements of MR contrast properties of MWCNT dispersions

Multiwalled carbon nanotubes (prepared using 600, 400, 200 and 60 mg of ferrocene catalyst) were dispersed in water containing Pluronic F127 (1% w/v) by horn sonication for 15 min. Next, the MWCNTs were diluted to final concentrations of 0.05, 0.06, 0.07, 0.08, 0.09, 0.1, 0.2 or 0.3 mg/ml in water, placed in a plastic holder, and their T2-weighted contrast enhancement properties were assessed using a 1.5 T GE Signa® MR scanner. The four preparations of MWCNTs were arranged in four rows with increasing concentration from left to right. Figure 1A shows a coronal MR image of representative MWCNTs in water. The modified spin echo pulse sequence was able to obtain a 1D projection image from each individual row by exciting each row separately. To measure T2, 128 1D projection images (field of view 32 cm, 128 points) were obtained from each slice. Each projection image was acquired with a different echo time (TE), which varied logarithmically from 14 ms to 14 s. The repition time (TR) was fixed at 15 s regardless of the TE. Total acquisition time was approximately 30 min. For each MCWNT preparation, the 1D projection images were concatenated together to form a TE time series. The time series for each preparation was fit to a single exponential decay curve in Matlab (MathWorks, MA, USA). After the TE for each MWCNT was measured, the relaxivity of each preparation was determined by linear least squares fitting of the R2 ($1/T_2$) as a function of the iron concentration in each MWCNT dispersion (Figure 1B).

Cell culture

Murine renal carcinoma cells were a gift from Robert Wiltrout (National Cancer Institute, MD, USA). Cells were grown in Roswell Park Memorial Institute media supplemented with 10% fetal bovine serum and 1% penicillin/streptomycin (Invitrogen, CA, USA). MDA-

MB-231 human breast adenocarcinoma cells were obtained from the American Type Culture Collection and grown in Dulbecco's Modified Eagle's medium supplemented with 10% fetal bovine serum, penicillin/streptomycin, and L-glutamine (Invitrogen, CA, USA).

Animal handling

All animal studies were performed in compliance with the institutional guidelines on animal use and welfare (Animal Care and Use Committee of Wake Forest University Health Sciences) under an approved protocol. Female Nu/Nu mice were purchased from Charles River Laboratories (MA, USA). Mice were housed in individually ventilated cages in groups of five under specific pathogen-free conditions and were allowed access to food and water *ad libitum*.

Kidney tumor animal model for tumor regression study

Murine renal carcinoma fragments were implanted into the right flanks of 12 female Nu/Nu mice and mice were randomized into three groups: control, vehicle and MWCNT. Once tumors reached a diameter of approximately 6 mm, 50 μl of a 2.0 mg/ml $MWCNT_{600}$ solution was injected directly into tumors of the MWCNT group. Controls were injected with an equal volume of vehicle. The next day, tumors of the vehicle and MWCNT groups were irradiated using a 1064 nm NIR laser beam (IPG Photonics) at 3 W/cm^2 (spot diameter = 5.5 mm) for 30 s. The laser beam was directed at the center of each tumor. Tumor growth was monitored with calipers and tumor volume calculated using the formula $(4/3)\pi(x/2)(y/2)(z/2)$.

Breast tumor animal model for MR T2 relaxation time measurement

Human breast adenocarcinoma cells, MDA-MB231 (American Type Culture Collection), were grown to log phase in 15-cm tissue culture dishes (Corning Costar, Lowell, MA, USA). Cells then were treated with trypsin-EDTA (Invitrogen), washed in phosphate-buffered saline (Invitrogen) and resuspended at a concentration of 2×10^7 cells/ml in a 1:1 mixture of Matrigel (BD Biosciences, San Jose, CA, USA) and phosphate-buffered saline. A total of 100 μl of the cell suspension was injected into the 4th inguinal mammary fat pad. Tumor growth was measured over time using calipers. When the two largest perpendicular diameters reached 8–10 mm, tumors were injected with the CNT suspension and imaged by MR.

7T high-resolution 3D T2 maps scan in a 7T Bruker micro-MRI scanner

In vivo T2 measurements were performed using a 7T Bruker Biospin® MicroMRI scanner. The scanner was equipped with a BGA-6S 60-mm inside diameter gradient and shim coil (max gradient 1000 mT/m; Bruker Daltonics, MA, USA). Two breast tumor-bearing mice were injected intratumorally with 50 μl of a 2 mg/ml suspension of $MWCNT_{600}$ or nitrogen-doped MWCNT ($MWCNT_{N\text{-}Doped}$). Mice were anesthetized with isoflurane during the MR scan. Tumor-bearing mice were positioned in a 35-mm Bruker quandrature birdcage volume coil to acquire high-resolution and signal-to-noise ratio MRI images. MR images were acquired using a multislice multiecho pulse sequence with slices positioned across the mouse tumor with the following parameters: TE = 10, 20, 30 … 160 ms, TR = 2000 ms, field of view = 3 × 3 cm, pixel size = 0.23 × 0.23 mm. A total of 16 MR images with different TEs were fit into an exponential decay equation to generate the 2D T2 maps. Mice were scanned using the T2 map MRI protocol described previously at five different time points: before MWCNTs injection, after MWCNTs injection, after laser treatment (3 W/cm^2, 30 s, NIR with wavelength = 1064 nm), 1 h after laser treatment, 24 h after laser treatment and 1 week post-treatment.

Results

Iron content of MWCNTs can be controlled at manufacture

Synthesis of MWCNTs was accomplished by chemical vapor deposition with ferrocene as a catalyst. During this process, iron particles are deposited in the nanotubes. These iron-containing MWCNTs are hollow tube-like structures that consist of multiple concentric layers of graphenic carbon with typical diameters in the range of 10–50 nm and length of approximately 1000 nm. By introducing increasing masses of ferrocene (60, 200, 400 and 600 mg) during synthesis, we hypothesized that more iron would become entrapped in the nanotubes. Although ferrocene is being investigated as an anticancer agent [29,30], some concern exists regarding potential toxicity following chronic exposure to ferrocene [31,32]. Therefore, MWCNTs were washed by ultrasonication for 20 h in sulfuric and nitric acid (3:1) following synthesis to eliminate iron contaminants on the outside, reducing any potential toxic side effects and ensuring that the ferrocene would remain colocalized with the MWCNTs. Analysis of the tubes by transmission electron microscopy (Figure 2) clearly shows iron particles entrapped inside the tubes, with no evidence of iron particles observed outside of the tubes. Inductively coupled plasma elemental analysis of the MWCNT preparations confirmed that the amount of iron encased in the MWCNTs was linearly related ($r = 0.983$) to the mass of ferrocene catalyst used during synthesis (Table 1). Throughout this article, the four types of nanotubes produced by this method are labeled $MWCNT_{60}$, $MWCNT_{200}$, $MWCNT_{400}$ or $MWCNT_{600}$ to indicate the mass of ferrocene present during synthesis (Table 1).

MR contrast properties of iron-containing MWCNTs are related to their iron content

Next, we dispersed these four different preparations of iron-containing MWCNTs ($MWCNT_{60, 200, 400, 600}$) in water at increasing concentrations (0.05, 0.06, 0.07, 0.08, 0.09, 0.1, 0.2 and 0.3 mg/ml) and assessed their T2-weighted contrast enhancement properties using a GE MR Signa HDx 1.5 T scanner. Analysis was conducted using an in-house modified spin-echo pulse sequence and the relaxivity of each preparation was determined as described in the 'Materials and methods' section. The efficiency of change in the relaxation properties (R_2) in tissue upon injection of a T2-weighted contrast agent is a function of the concentration (M) of the effective superparamagnetic materials as described by Equation 1:

$$\left(\frac{1}{T_2}\right)_{total} = \left(\frac{1}{T_2}\right)_0 + M \cdot R_2$$

where $(1/T_2)_{total}$ is the relaxation rate in the presence of a contrast agent, and $(1/T_2)_{0\ is}$ the relaxation rate without the contrast agent.

Figure 1A shows a coronal MR image of MWCNTs produced using the lowest ($MWCNT_{60}$) and highest ($MWCNT_{600}$) concentrations of iron in water. As shown in Figure 1B, R_2 properties were dependent on iron content of the MWCNTs, with higher iron content associated with increasing R_2 relaxivity ($r^2 = 0.72$).We tested the stability of contrast enhancement by monitoring the T2 relaxation properties of a dispersion of $MWCNT_{60}$. $MWCNT_{60}$ was diluted to final concentrations of 0.4, 0.3, 0.2, 0.1, 0.09, 0.08, 0.07, 0.06, 0.05 and 0.04 mg/ml and T2 relaxivities were measured periodically over 5 days. During this time, some of the tubes sedimented and the nanotube concentration visibly increased at the bottom of the tube and decreased at the top. Due to sedimentation of $MWCNT_{60}$, apparent R_2 in the upper half of the tube fell from an initial value of 0.129–0.106 ms^{-1}/mg/ml by day 2, and further dropped to 0.062 ms^{-1}/mg/ml by day 5. However, following mild shaking to disperse the $MWCNT_{60}$, the measured contrast enhancement ($R_2 = 0.128$ ms^{-1}/

mg/ml) was virtually unchanged from the initial measurement prior to sedimentation, indicating that imaging properties of MWCNTs are stable over time and may potentially be used to monitor MWCNT concentration.

Iron content does not influence heating properties of MWCNTs following exposure to NIR

As we and others have previously reported, the ability of MWCNTs to act as thermal ablation agents is dependent on their ability to induce a temperature increase following stimulation with NIR radiation [13,19]. To determine if the heating property of the MWCNTs was affected by the iron content of MWCNTs, we measured the temperature increase of dispersions of MWCNTs with variable iron content following exposure to NIR. We prepared 100 μg/ml suspensions of four different types of iron-containing nanotubes ($MWCNT_{60,200,400,600}$) in water, then exposed them to a Nd:YAG laser generating 1064 nm NIR with a fluence of 3 W/cm^2 for 30, 60 or 90 s. In parallel, we also tested $MWCNT_{N\text{-}Doped}$, which do not contain iron and which we previously demonstrated to be effective heat tranducers for LITT [33]. Temperatures were measured directly by thermocouple. As shown in Figure 3, all MWCNT types produced similar temperature increases, regardless of iron content, increasing from 26°C to greater than 42°C after 30 s of NIR exposure. Longer durations of irradiation resulted in even greater final temperatures, but no significant differences were observed between nanotubes differing in iron content, regardless of irradiation time.

Iron-containing MWCNTs are effective agents for tumor ablation

We previously demonstrated that injection of 100 μg of $MWCNT_{N\text{-}Doped}$ into a murine renal tumor implanted on a mouse flank followed by 30 s of low-energy NIR exposure was effective at preventing tumor growth and inducing long-term (>180 days) remission in 80% of the treated mice [19]. Because $MWCNT_{600}$ were the most efficient contrast agent of the four types of iron-containing nanotubes tested (Figure 1), we next confirmed that $MWCNT_{600}$ were effective mediators for LITT of cancer *in vivo* using the same cancer model and the most effective treatment parameters determined in our earlier study (Figure 4) [19]. A total of 12 nude mice were inoculated with murine renal carcinoma tumor fragments in the flanks. When the tumors reached an average diameter of 6 mm, the mice were randomized into three groups (n = 4 per group): 'untreated', 'vehicle and laser' and '100 μg MWCNT and laser.' Tumors in the 'vehicle and laser' and '100 μg MWCNT and laser' groups were injected with saline or 100 μg $MWCNT_{600}$, respectively. Tumors in these groups were then illuminated with NIR at 3 W/cm^2 for 30 s and treatment-induced changes in tumor volume were tracked by daily caliper measurements. The 'untreated' control group received no intervention. The study was concluded 2 weeks post-treatment when the tumor volume on the mice from the untreated and vehicle control groups exceeded the predetermined 1000 mm^3 threshold for humane euthanasia. Following treatment, tumors in the untreated and vehicle control groups displayed exponential growth and achieved group mean tumor volumes of 1248 mm^3 (± 423) and 1393 mm^3 (± 441), respectively. These values were not statistically different ($p = 0.681$). By contrast, mice treated with the combination of 100 μg $MWCNT_{600}$ and NIR laser radiation had a significantly decreased mean tumor volume (90 mm^3 ±146) relative to untreated controls ($p < 0.0025$). Thus, iron-containing MWCNTs are effective mediators of LITT in an *in vivo* model of cancer.

Laser treatment does not affect heating or MR contrast properties of iron-containing MWCNTs

A potential advantage of MWCNTs as tumor ablative (and MR contrast) agents is their ability to remain resident in the tumor tissue over time following therapeutic administration [19]. This property may allow both multiple treatments and the collection of successive MR images without the need for injection of new contrast agents. In order for this capability to

be exploited, the thermal and MR properties of MWCNTs must remain stable following multiple cycles of NIR exposure. To test this, we initially subjected suspensions of MWCNTs to multiple cycles of laser treatment and measured temperature increases. The heating properties of all MWCNT preparations remained stable after three cycles of heating and cooling (Figure 5).

We then tested the effect of laser irradiation on contrast properties and stability of iron-containing MWCNTs *in vivo*. Because image-guided LITT is used clinically for treatment of breast cancer [34], we used an orthotopic mouse model of human breast cancer in these experiments. Two nude mice were injected in the 4th inguinal mammary fat pad with the human breast adenocarcinoma cell line, MDA-MB-231. To prevent these tumors from undergoing complete remission following MWCNT-mediated LITT, we allowed them to achieve a diameter of 8–10 mm before beginning treatment. Since the laser beam diameter was only 5 mm, leading to partial but not complete tumor ablation, this model allowed for repeated imaging of the treatment area. Baseline images of each tumor were collected using a Bruker 7T micro-MRI scanner. Tumors were then injected with either 100 μg of $MWCNT_{600}$ or MR-invisible $MWCNT_{N\text{-}Doped}$ for direct comparison. Tumors were reimaged by MR to determine the MWCNT distribution and then mice were treated by image-guided LITT. The MR images show that the iron-containing MWCNTs were distributed throughout the tumor volume, but only the area illuminated by the laser was ablated, suggesting that MR imaging may be useful for accurately guiding such therapy (Figure 6). The calculated T2 relaxation time of the tumor dropped from 61 ms prior to iron-containing MWCNT injection to 22 ms after injection. By contrast, in the $MWCNT_{N\text{-}Doped}$ treated mouse, the T2 relaxation time was calculated as 60 ms both before and after the injection with nanoparticles, indicating that iron content is essential for this contrast enhancement. Furthermore, iron-containing MWCNTs were clearly visible in the tumor at 10 min, 24 h and 1 week after LITT and the T2 relaxation time at the site of injection remained near 20 ms for the duration of the study, indicating that MWCNT chemical decomposition and migration is minimal up to 1 week after injection, and suggesting that repeated treatment of the same site may be feasible using such nanotubes for image-guided LITT.

Discussion

In an effort to improve heating efficiency and localization of LITT, several investigations into the use of metallic and carbon-based nanomaterials as transducers of NIR have been conducted [6,8,13,35–37]. Others have shown that SWCNTs that have been modified to incorporate gadolinium-based MR contrast agents can be detected by MRI [22]. Furthermore, metal impurities trapped between bundles of SWCNT can also be detected by MRI [22]. However, to our knowledge, no information on the MR contrast properties of MWCNTs is available. As MWCNTs may have improved thermal ablation properties relative to SWCNTs [19], we examined whether MWCNTs could be used for combined MRI and nanoparticle-assisted LITT for cancer treatment. Since covalent functionalization of CNTs may alter their electrical and thermal properties, reducing their effectiveness as thermal ablation agents, we investigated strategies that would permit the incorporation of known MRI contrast agents, such as iron, into the MWCNTs during the growth phase. Chemical vapor deposition, which uses iron-containing ferrocene as a growth catalyst, allows for the synthesis of MWCNTs with superparamagnetic iron entrapped within their central lumen. Furthermore, iron oxide is a superparamagnetic material that enhances the MR image contrast by shortening the T2 relaxation time of the tissue surrounding the region into which it is delivered [23–28]. Although we did not directly test the magnetic properties of the MWCNTs used in these experiments, others have suggested that iron-containing CNTs possess magnetic properties [8,38]. Therefore, we developed iron-containing

MWCNTs and tested their applicability for combined MWCNT-assisted/mediated LITT and MR tumor imaging.

MRI-guided LITT is showing increasing promise as a technique for the treatment of a variety of primary and secondary malignant tumors [39–42]. Yet, despite its efficacy in well-selected patients, image-guided LITT is still far less frequently used than RF ablation techniques due to an inability to generate sufficiently high, tumor-specific heating [43]. Typically, lasers used for LITT are tuned to the NIR spectrum due to an absence of endogenous chromophores that absorb in this spectral region [44]. NIR can achieve tissue penetration depths of up to 6 cm, sufficient to treat breast, prostate, skin and head and neck cancers with an external laser source. However, precisely because of the inefficiency in energy absorption at this wavelength, it is difficult to deliver laser energy sufficient to generate thermoablative temperatures to depths beyond those considered superficial without damaging the intervening tissue. Similarly, it is difficult to confine the treatment area for large tumors (size >1 cm^3) without causing considerable damage to neighboring tissue. Therefore, development of nanomaterials capable of absorbing NIR and efficiently converting it into heat to generate thermoablative temperatures following a brief exposure to NIR can greatly expand the clinical use of LITT by confining the treatment to the area into which the nanomaterial has been delivered.

We recently demonstrated that, compared with other nanomaterials, MWCNTs enable more efficient conversion of NIR energy into heat, leading to durable tumor remission in mouse models of cancer [19]. In the present study, we further demonstrate that when engineered to contain iron, MWCNTs have favorable MR contrast enhancement properties, and that these nanoparticles have potential for use as dual-modality agents for T2 MR contrast imaging and MR image-guided LITT. MR images (Figure 6) show that MWCNTs injected into tumors and treated with NIR remain at the injection site for at least 1 week following laser irradiation. Thus, because the distribution of the MWCNTs can be monitored over time, multiple or fractionated laser treatments could be targeted to the tumor as necessary without the need for additional injections. This offers another advantage over RF ablation, which requires direct insertion of the RF probe with each treatment. Furthermore, MRI provides an accurate picture of the distribution of these efficient NIR transducers inside the tumor, which is essential information for pretreatment planning and determination of laser positioning.

Our previous studies indicate that in tumors injected with MWCNTs, temperatures of up to 70°C can be achieved at the site of nanotube injection following a 30-s exposure to NIR, over 30°C greater than the temperature rise observed in the absence of MWCNTs [19]. However, in cases where the tumor volume exceeds the area of nanotube coverage, or following incomplete treatment of a tumor such that the periphery continues to grow after the initial treatment (as seen in Figure 6), careful treatment planning will be necessary to ensure that if repeat treatments are applied, sufficient heat diffuses from the site of the nanotubes to the tumor periphery to completely eradicate the tumor. Mathematical modeling of heat transfer and MR thermometry will be essential tools in future investigations to determine energy delivery parameters that optimize heat delivery to the treated area while minimizing temperature increases in neighboring or intervening healthy tissue.

The potential toxicity of nanomaterials remains a concern for further clinical development. As more information becomes available, it is clear that CNT exposure can lead to many different toxicological outcomes depending upon characteristics of the material, including size, shape, surface chemistry, surface charge and agglomeration state [45–47]. Although we did not note any acute toxicity during our *in vivo* studies, more detailed toxicological,

pharmacokinetic and pharmocodynamic analysis will be required. The ability to track iron-containing MWCNTs by MR may offer considerable insight into their *in vivo* behavior.

Conclusion

Clinical application of nanoparticle-assisted LITT will require the use of a compatible imaging modality to spatially define the margins of the target lesion, assess the distribution of injected nanoparticles within the tumor, and ensure the appropriate thermal dose was achieved in the target area. Here we demonstrate that iron-containing MWCNTs are bifunctional nanoparticles, capable of being located by MRI and also effective as transducers of LITT. This combined functionality allows these nanoparticles to overcome some of the drawbacks of traditional thermotherapy. Refinement of the nanoparticle-mediated, image-guided LITT introduced here may allow expanded clinical use of image-guided LITT and improve therapeutic outcomes for cancer patients following such treatment.

Future perspective

Interest in the biomedical application of nanotubes has stemmed not only from their unusual physico–chemical properties, but from their potential to serve multiple functions simultaneously. For example, in this article we suggest that iron-containing MWCNTs have utility in the simultaneous imaging and therapy of tumors. Carbon nanotubes can also be engineered to concurrently deliver genes, drugs, and imaging agents. Over the next 5–10 years, we envision the continued evolution and refinement of these materials. With appropriate assessment of efficacy, biodistribution and toxicology, the potential for novel clinical applications is high.

Executive summary

- Iron-containing multiwalled carbon nanotubes (MWCNTs) were generated for combined tumor-specific thermal ablation and MRI contrast.
- Iron-containing MWCNTs were effective magnetic resonance contrast agents; contrast enhancement was proportional to iron content.
- Iron-containing MWCNTs generated thermoablative temperatures following exposure to near infared (NIR) radiation.
- MWCNTs retained their MR contrast properties following exposure to NIR radiation and could be used to longitudinally track MWCNTs.
- Treatment of tumor-bearing mice with iron-containing MWCNTs and NIR radiation led to a significant reduction in tumor burden.
- This is the first study to demonstrate the use of iron-containing MWCNTs as bifunctional nanomaterials for the imaging and treatment of cancer.

Acknowledgments

We thank the Center for Biomolecular Imaging at Wake Forest University School of Medicine (NC, USA) for assistance with the 7T Bruker micro-MRI scanner and the Microscopy Core of the Comprehensive Cancer Center for the transmission electron microscope and light microscope.

This work was supported in part by National Institutes of Health Grant RO1CA12842 (SVT). Ravi Singh was supported, in part, by training grant T32CA079448.

Bibliography

Papers of special note have been highlighted as:

▪ of interest

1. Wagner V, Dullaart A, Bock AK, Zweck A. The emerging nanomedicine landscape. Nat. Biotechnol. 2006; 24(10):1211–1217. [PubMed: 17033654]
2. Lacerda L, Raffa S, Prato M, Bianco A, Kostarelos K. Cell-penetrating CNTs for delivery of therapeutics. Nano. Today. 2007; 2(6):38–43.
3. Raffa V, Ciofani G, Nitodas S, et al. Can the properties of carbon nanotubes influence their internalization by living cells? Carbon. 2008; 46(12):1600–1610.
4. Singh R, Pantarotto D, McCarthy D, et al. Binding and condensation of plasmid DNA onto functionalized carbon nanotubes: toward the construction of nanotube-based gene delivery vectors. J. Am. Chem. Soc. 2005; 127(12):4388–4396. [PubMed: 15783221]
5. Shi DL. Integrated multifunctional nanosystems for medical diagnosis and Treatment. Adv. Func. Mater. 2009; 19(21):3356–3373.
6. Avedisian CT, Cavicchi RE, Mceuen PL, Zhou X. Nanoparticles for cancer treatment: role of heat transfer. Ann. NY Acad. Sci. 2009; 1161:62–73. [PubMed: 19426306]
7. Harris DL, Bawa R. The carbon nanotube patent landscape in nanomedicine: an expert opinion. Expert Opin. Ther. Pat. 2007; 17(9):1165–1174.
8. Klingeler R, Hampel S, Buchner B. Carbon nanotube based biomedical agents for heating, temperature sensoring and drug delivery. Int. J. Hyperthermia. 2008; 24(6):496–505. [PubMed: 18923989]
9. Kostarelos K, Bianco A, Prato M. Promises, facts and challenges for carbon nanotubes in imaging and therapeutics. Nat. Nanotechnol. 2009; 4(10):627–633. [PubMed: 19809452] ▪ Current knowledge of *in vivo* applications of carbon nanotubes for cancer offering insight into future strategies for rational development of nanotube-based theranostics.
10. Murday JS, Siegel RW, Stein J, Wright JF. Translational nanomedicine: status assessment and opportunities. Nanomedicine: NBM. 2009; 5(3):251–273.
11. Portney NG, Ozkan M. Nano-oncology: drug delivery, imaging, and sensing. Anal. Bioanal. Chem. 2006; 384(3):620–630. [PubMed: 16440195]
12. Teker K. Bioconjugated carbon nanotubes for targeting cancer biomarkers. Mater. Sci. Eng. B. 2008; 153(1–3):83–87.
13. O'Neal DP, Hirsch LR, Halas NJ, Payne JD, West JL. Photo-thermal tumor ablation in mice using near infrared-absorbing nanoparticles. Cancer Lett. 2004; 209(2):171–176. [PubMed: 15159019] ▪ An early study on nanoparticle-assisted laser-induced thermotherapy demonstrating that complete tumor remission can be achieved in tumor-bearing mice treated with gold nanoshells and near infrared radiation.
14. Kangasniemi M, McNichols RJ, Bankson JA, Gowda A, Price RE, Hazle JD. Thermal therapy of canine cerebral tumors using a 980 nm diode laser with MR temperature-sensitive imaging feedback. Lasers Surg. Med. 2004; 35(1):41–50. [PubMed: 15278927]
15. Nikfarjam M, Muralidharan V, Christophi C. Mechanisms of focal heat destruction of liver tumors. J. Surg. Res. 2005; 127(2):208–223. [PubMed: 16083756]
16. Manthe RL, Foy SP, Krishnamurthy N, Sharam B, Labhasetwar VD. Tumor ablation and nanotechnology. Mol. Pharm. 2010 ▪ Various types of nonsurgical tumor ablation methods currently used in clinical cancer treatment and the potential improvements offered by application of nanotechnology.
17. Ryan TP, Turner PF, Hamilton B. Interstitial microwave transition from hyperthermia to ablation: historical perspectives and current trends in thermal therapy. Int. J. Hyperthermia. 2010; 26(5): 415–433. [PubMed: 20597625]
18. Widmann G, Bodner G, Bale R. Tumour ablation: technical aspects. Cancer Imaging. 2009; 9(Spec. No A):S63–S67. [PubMed: 19965296]

19. Burke A, Ding X, Singh R, et al. Long-term survival following a single treatment of kidney tumors with multiwalled carbon nanotubes and near-infrared radiation. Proc. Natl Acad. Sci. USA. 2009; 106(31):12897–12902. [PubMed: 19620717] ▪ Our previous study demonstrated that treatment of tumor-bearing mice with multiwalled carbon nanotubes (MWCNTs) and near infrared radiation leads to long-term tumor remission without relapse and demonstrated by magnetic resonance thermometry that the thermal treatment is largely confined to the site of MWCNT injection.
20. Chen WR, Korbelik M, Bartels KE, Liu H, Sun J, Nordquist RE. Enhancement of laser cancer treatment by a chitosan-derived immunoadjuvant. Photochem. Photobiol. 2005; 81(1):190–195. [PubMed: 15535737]
21. Gnyawali SC, Chen Y, Wu F, et al. Temperature measurement on tissue surface during laser irradiation. Med. Biol. Eng. Comput. 2008; 46(2):159–168. [PubMed: 17891430]
22. Al Faraj A, Cieslar K, Lacroix G, Gaillard S, Canot-Soulas E, Cremillieux Y. *In vivo* imaging of carbon nanotube biodistribution using magnetic resonance imaging. Nano. Letters. 2009; 9(3): 1023–1027. [PubMed: 19199447]
23. Bomatí-Miguel O, Morales MP, Tartaj P, et al. Fe-based nanoparticulate metallic alloys as contrast agents for magnetic resonance imaging. Biomaterials. 2005; 26(28):5695–5703. [PubMed: 15878375]
24. Bulte JWM, Kraitchman DL. Iron oxide MR contrast agents for molecular and cellular imaging. NMR Biomed. 2004; 17(7):484–499. [PubMed: 15526347]
25. Cunningham CH, Arai T, Yang PC, Mcconnell MV, Pauly JM, Conolly SM. Positive contrast magnetic resonance imaging of cells labeled with magnetic nanoparticles. Magn. Reson. Med. 2005; 53(5):999–1005. [PubMed: 15844142]
26. Fahlvik AK, Klaveness J, Stark DD. Iron oxides as MR imaging contrast agents. J Magn. Reson. Imaging. 1993; 3(1):187–194. [PubMed: 8428086]
27. Mani V, Briley-Saebo KC, Itskovich VV, Samber DD, Fayad ZA. Gradient echo acquisition for superparamagnetic particles with positive contrast (GRASP): sequence characterization in membrane and glass superparamagnetic iron oxide phantoms at 1.5T and 3T. Magn. Reson. Med. 2006; 55(1):126–135. [PubMed: 16342148]
28. Saini S, Stark DD, Hahn PF, Wittenberg J, Brady TJ, Ferrucci JT Jr. Ferrite particles: a superparamagnetic MR contrast agent for the reticuloendothelial system. Radiology. 1987; 162(1 Pt 1):211–216. [PubMed: 3786765]
29. Kovjazin R, Eldar T, Patya M, Vanichkin A, Lander HM, Novogrodsky A. Ferrocene-induced lymphocyte activation and antitumor activity is mediated by redox-sensitive signaling. FASEB. J. 2003; 17(1):467–469. [PubMed: 12514114]
30. Ferle-Vidovic A, Potjak-Blazi M, Rapic V, Skare D. Ferrocenes (F168, F169) and fero-sorbitol-citrate (FSC): potential anticancer drugs. Cancer. Biother. Radiopharm. 2000; 15(6):617–624. [PubMed: 11190493]
31. Schechter B, Caldwell G, Neuse EW. A preliminary study of the toxicological properties of selected polymer-ferrocene conjugates. J. Inorg. Organomet. Polymer Mater. 2000; 10(4):177–188.
32. Nikula KJ, Sun JD, Barr EB, et al. 13-week, repeated inhalation exposure of F344/N rats and B6c3f1 mice to ferrocene. Fundam. Appl. Toxicol. 1993; 21(2):127–139. [PubMed: 8405775]
33. Torti SV, Byrne F, Whelan O, et al. Thermal ablation therapeutics based on CNx multi-walled nanotubes. Int. J. Nanomedicine. 2007; 2(4):707–714. [PubMed: 18203437]
34. Dowlatshahi K, Dieschbourg JJ, Bloom KJ. Laser therapy of breast cancer with 3-year follow-up. Breast J. 2004; 10(3):240–243. [PubMed: 15125752]
35. Huang HC, Rege K, Heys JJ. Spatiotemporal temperature distribution and cancer cell death in response to extracellular hyperthermia induced by gold nanorods. ACS Nano. 2010; 4(5):2892–2900. [PubMed: 20387828]
36. Park JH, Von Maltzahn G, Xu MJ, et al. Cooperative nanomaterial system to sensitize, target, and treat tumors. Proc. Natl Acad. Sci. USA. 2010; 107(3):981–986. [PubMed: 20080556]
37. Day ES, Morton JG, West JL. Nanoparticles for thermal cancer therapy. J. Biomech. Eng. 2009; 131(7) 074001.

38. Krupskaya Y, Mahn C, Parameswaran A, et al. Magnetic study of iron-containing carbon nanotubes: feasibility for magnetic hyperthermia. J. Magn. Magn. Mater. 2009; 321(24):4067–4071.
39. Mack MG, Straub R, Eichler K, et al. Percutaneous MR imaging-guided laser-induced thermotherapy of hepatic metastases. Abdom. Imaging. 2001; 26(4):369–374. [PubMed: 11441548]
40. Mack MG, Straub R, Eichler K, Sollner O, Lehnert T, Vogl TJ. Breast cancer metastases in liver: laser-induced interstitial thermotherapy – local tumor control rate and survival data. Radiology. 2004; 233(2):400–409. [PubMed: 15459328]
41. Mack MG, Vogl TJ. MR-guided ablation of head and neck tumors. Neuroimaging Clin. N. Am. 2004; 14(4):853–859. [PubMed: 15489155]
42. Meister D, Hubner F, Mack M, Vogl TJ. MR thermometry for laser-induced thermotherapy at 1.5 tesla. Rofo. 2007; 179(5):497–505. [PubMed: 17436184]
43. Ferrari FS, Megliola A, Scorzelli A, et al. Treatment of small HCC through radiofrequency ablation and laser ablation. Comparison of techniques and long-term results. Radiol. Med. 2007; 112(3):377–393. [PubMed: 17447018]
44. Weissleder R. A clearer vision for *in vivo* imaging. Nat. Biotechnol. 2001; 19(4):316–317. [PubMed: 11283581]
45. Deng XY, Wu F, Liu Z, et al. The splenic toxicity of water soluble multi-walled carbon nanotubes in mice. Carbon. 2009; 47(6):1421–1428.
46. Qu GB, Bai YH, Zhang Y, Jia Q, Zhang WD, Yan B. The effect of multiwalled carbon nanotube agglomeration on their accumulation in and damage to organs in mice. Carbon. 2009; 47(8):2060–2069.
47. Yang ST, Wang X, Jia G, et al. Long-term accumulation and low toxicity of single-walled carbon nanotubes in intravenously exposed mice. Toxicol. Lett. 2008; 181(3):182–189. [PubMed: 18760340]

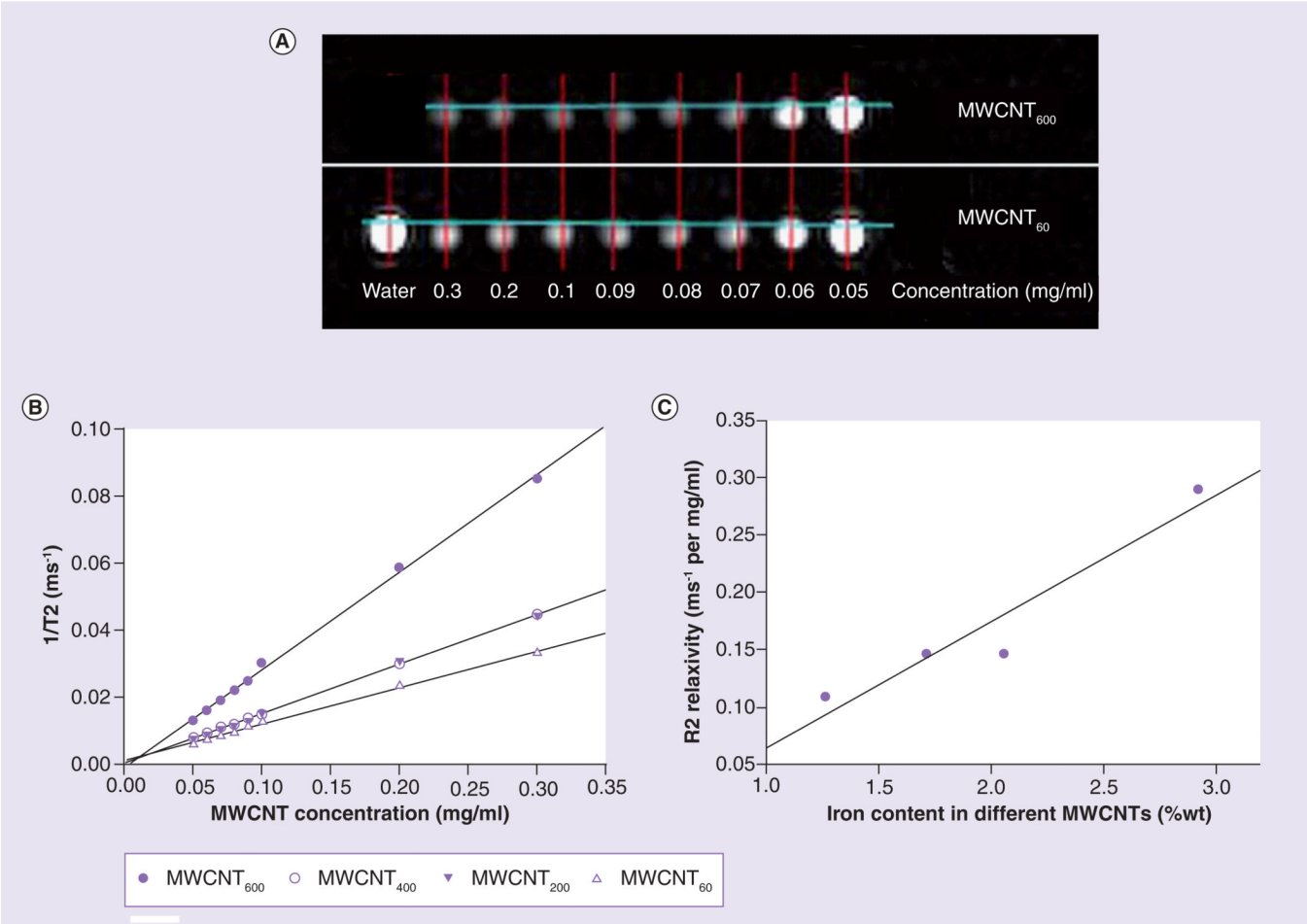

Figure 1. Magnetic resonance contrast properties of multiwalled carbon nanotubes are dependent on their iron content

(A) Four different preparations of MWCNTs that differed in iron content were diluted to final concentrations ranging from 0.05 to 0.3 mg/ml and imaged on a GE MR-Signa HDx 1.5T Scanner. MRI coronal images of MWCNTs fabricated using the highest ($MWCNT_{600}$) and lowest ($MWCNT_{60}$) concentrations of iron are shown. Test tubes containing water with different concentration of gadolinium were used as an asymmetric landmark (bottom row first tube), as well as a reference for validating T2 measurements. **(B)** 1/T2 versus MWCNT concentrations: $MWCNT_{600}$ are more effective contrast agents than MWCNTs prepared with lower iron concentrations as indicated by the steeper slope (R_2 relaxivity) of the curve. **(C)** R_2 value of MWCNT preparations as a function of actual iron content of the MWCNT preparations (Table 1). The data strongly indicate that increased iron content correlates with improved contrast enhancement ($r^2 = 0.72$).

MWCNT: Multiwalled carbon nanotubes.

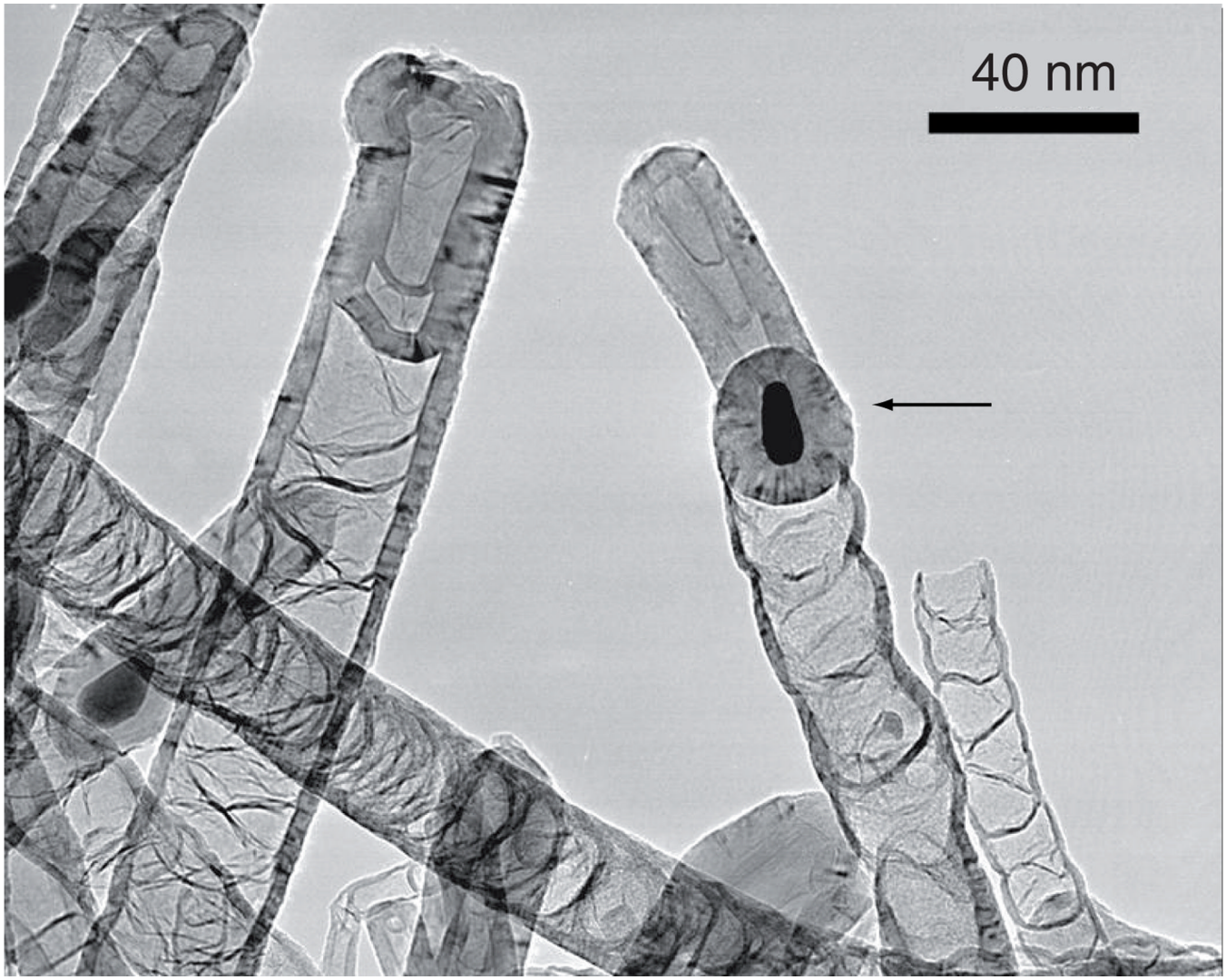

Figure 2. Transmission electron microscopy image of iron-containing multiwalled carbon nanotubes

Representative image of multiwalled carbon nanotubes (MWCNTs) grown using 200-mg ferrocene ($MWCNT_{200}$). Iron is visible as dark spots located inside the tubes (arrow).

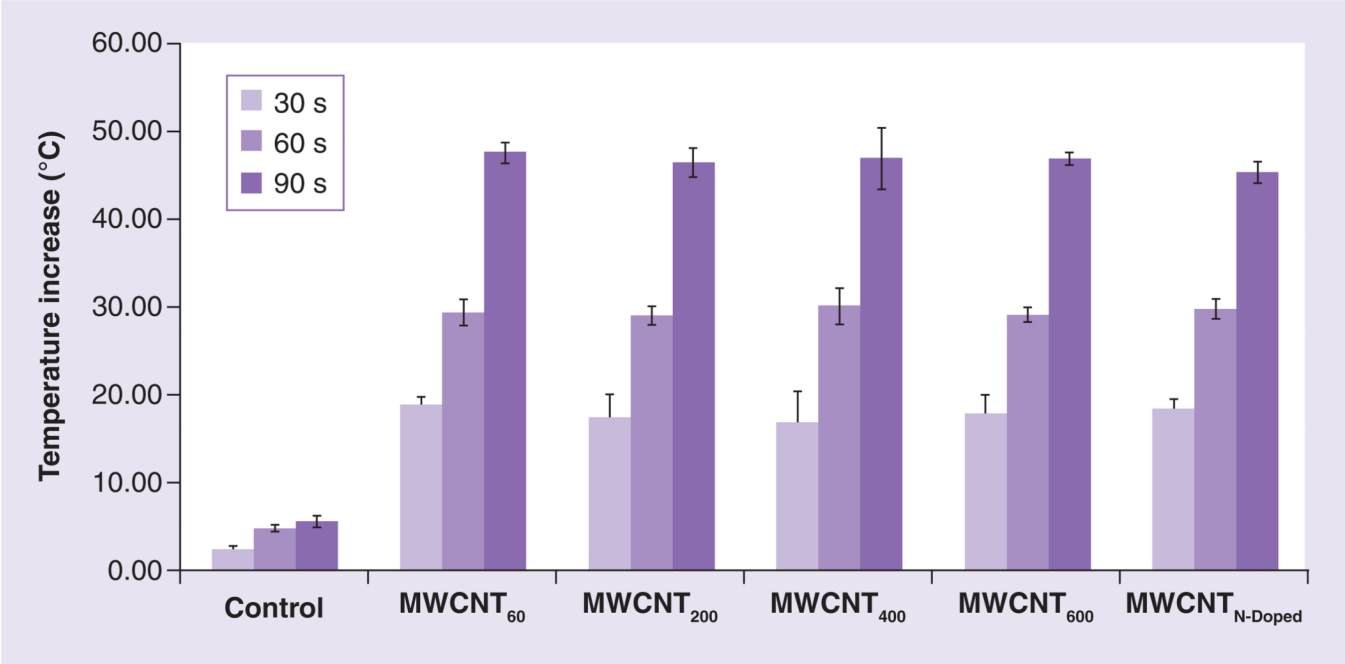

Figure 3. Increase in temperature following near infrared radiation irradiation of multiwalled carbon nanotubes is independent of their iron content

Iron-containing and N-Doped MWCNTs were suspended to a final concentration of 100 μg/ml, exposed to near infrared (NIR) laser at 3 W/cm^2 for 30, 60, 90 seconds. Temperature was measured prior to NIR exposure and post NIR exposure. Data indicate the increase in temperature over baseline following NIR treatment. Shown are means ± standard deviations of triplicate samples.

MWCNT: Multiwalled carbon nanotube; N-Doped: Nitrogen-doped.

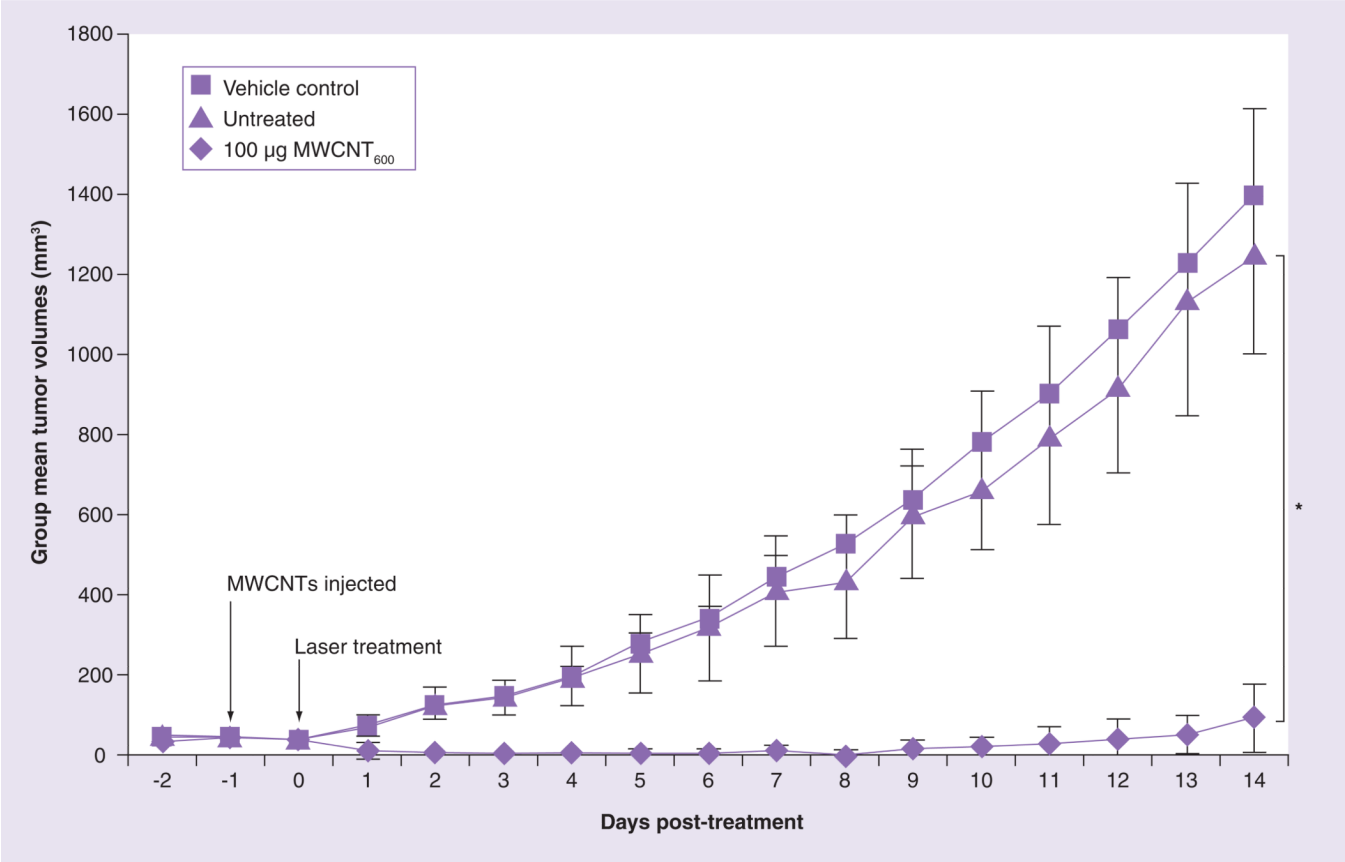

Figure 4. Iron-containing multiwalled carbon nanotubes are effective tumor ablative agents

Tumor-bearing mice were divided into three groups (n = 4 per group). Tumors were injected with either vehicle or 100 μg $MWCNT_{600}$. Control mice received no further treatment; $MWCNT_{600}$ and vehicle group were exposed to a 1064 nm NIR laser for 30 s. Tumor volumes were monitored over time and compared at the 14 day end point.

*Growth of tumors treated with the combination of $MWCNT_{600}$ and laser was statistically different from control ($p < 0.0025$, Student's t-test).

MWCNT: Multiwalled carbon nanotube.

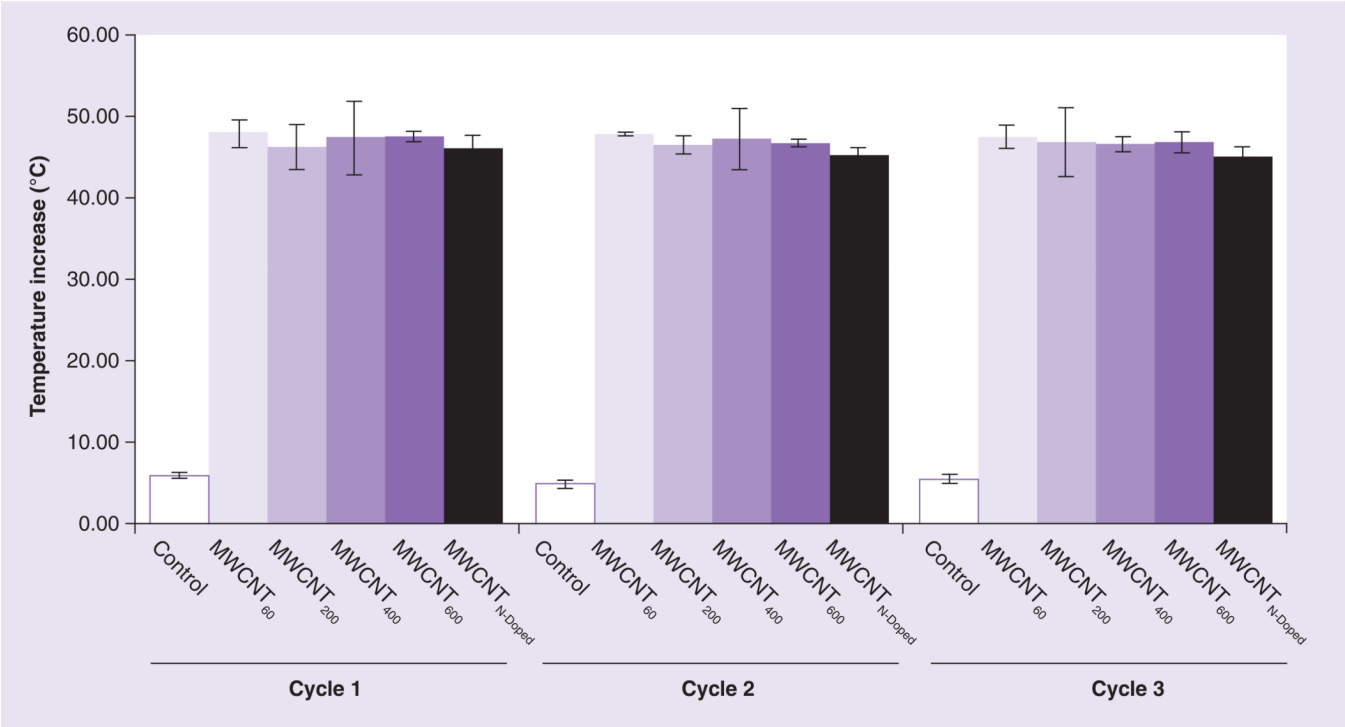

Figure 5. Multiple rounds of laser treatment do not affect the ability of multiwalled carbon nanotube preparations to induce an increase in temperature

Phosphate-buffered saline alone (control), MWCNTs of increasing iron content ($MWCNT_{60,200,400,600}$), or $MWCNT_{N\text{-}Doped}$ containing no iron were suspended at 100 μg/ml and exposed to near infrared (NIR) laser for 30 s Temperature was measured prior to NIR exposure and post NIR exposure. The preparations were allowed to cool to room temperature and NIR exposure and temperature measurements were repeated for two additional cycles. Data indicate the increase in temperature over baseline following NIR treatment. Shown are means ± standard deviations of triplicate samples.
MWCNT: Multiwalled carbon nanotube; N-Doped: Nitrogen-doped.

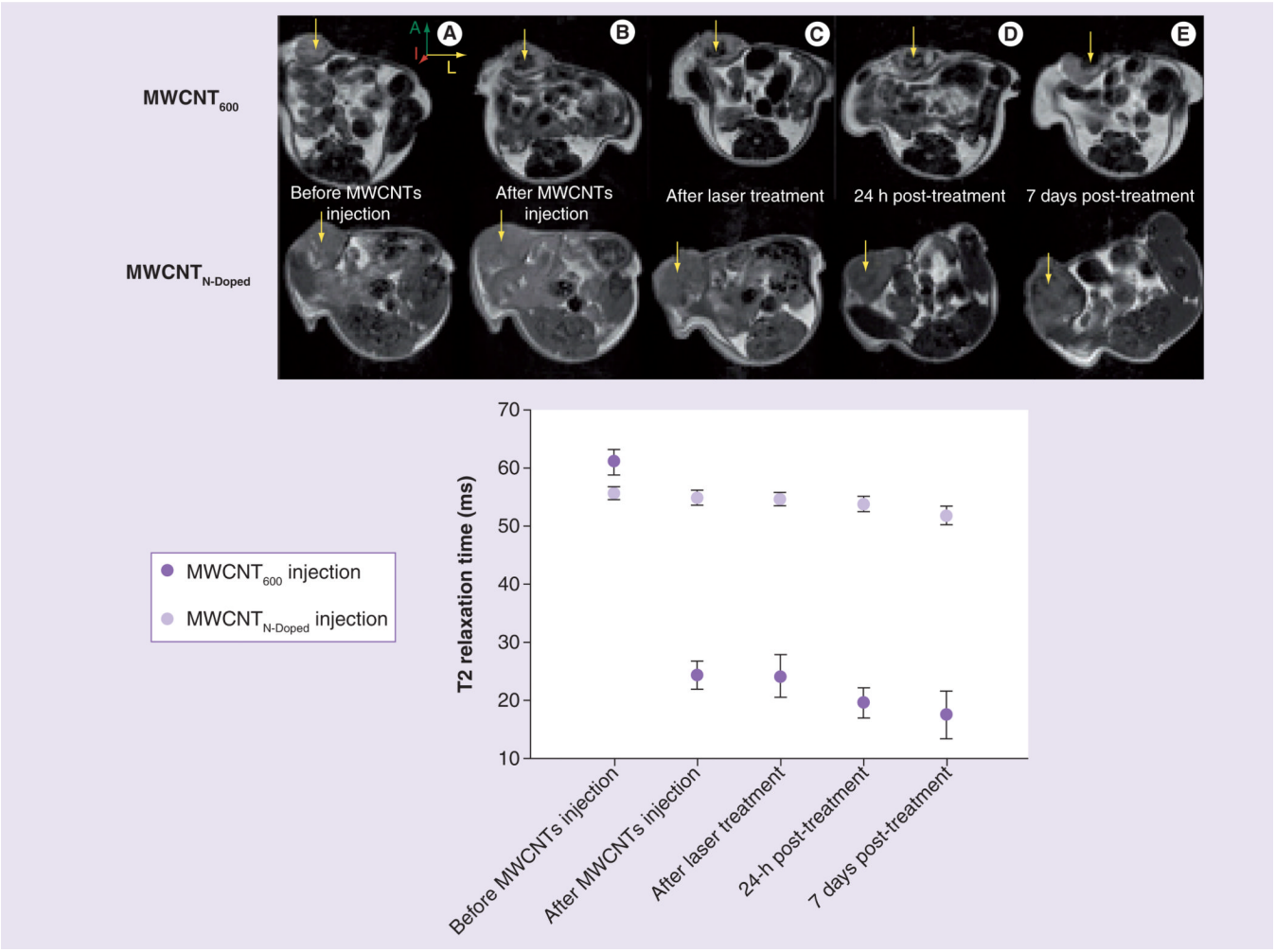

Figure 6. Magnetic resonance contrast properties of multiwalled carbon nanotubes are stable *in vivo*

(A) Representative axial MR images of two breast tumors injected with either 100 μg $MWCNT_{600}$ or $MWCNT_{N\text{-}doped}$ and subsequently exposed for 30 s to NIR laser. Arrows show the injection site. Images were collected at five timepoints: before injection, immediately after injection, immediately after laser treatment, 24 h after laser treatment, and 7 days after laser treatment (laser power: 3 W/cm^2, 1064 nm wavelength). **(B)** T2 relaxation measurement of the tumor region was acquired using multislice multipulse sequence at the five different time points described in **(A)**.

A: Anterior; I: Inferior; L: Left; MR: Magnetic resonance; MWCNT: Multiwalled carbon nanotube; N-Doped: Nitrogen-doped.

Table 1

Iron content of multiwalled carbon nanotube preparations.

MWCNT type	Mass of ferrocene catalyst used during manufacture (mg)	Iron concentration% (wt/wt)
$MWCNT_{600}$	600	2.92
$MWCNT_{400}$	400	2.05
$MWCNT_{200}$	200	1.71
$MWCNT_{60}$	60	1.26

MWCNT: Multiwalled carbon nanotube.